Vertex-corrected tunneling inversion in electron-phonon mediated superconductors: Pb

J. K. Freericks
Department of Physics, Georgetown University, Washington, D.C. 20057-0995

E. J. Nicol
Department of Physics, University of Guelph, Guelph, Ontario, Canada N1G 2W1

A. Y. Liu
Department of Physics, Georgetown University, Washington, D.C. 20057-0995

A. A. Quong
Sandia National Laboratories, Livermore, California 94551-0969

(Received 11 October 1996)

The McMillan-Rowell tunneling inversion program, which extracts the electron-phonon spectral function $\alpha^2F(\Omega)$ and the Coulomb pseudopotential μ^* from experimental tunneling data, is generalized to include the lowest-order vertex correction. We neglect the momentum dependence of the electron-phonon matrix elements, which is formally equivalent to using a local approximation. The perturbation theory is performed on the imaginary axis and then an exact analytic continuation is employed to produce the tunneling density of states on the real axis. Comparison is made with the experimental data for Pb. We find λ is increased by approximately 1% due to the vertex corrections. [S0163-1829(97)10817-7]

I. INTRODUCTION

The theory of low-temperature superconductors is one of the most accurate theories in condensed-matter physics. Agreement to better than one part in 10^4 is common between the tunneling density of states (DOS) measured experimentally and that calculated with an extracted electron-phonon spectral function $\alpha^2F(\Omega)$ and Coulomb pseudopotential μ^*. The reason why the agreement is so good is due to Migdal's theorem,[1] as formulated by Eliashberg[2] in the superconducting state, which says that there is a small parameter in the theory, namely the ratio of the phonon energy scale to the electronic energy scale, that guarantees the rapid convergence of the perturbative expansion. However, in some recently discovered materials that are thought to be electron-phonon superconductors, the ratio of the phonon to electronic energy scale is no longer as small. Two examples are $Ba_{1-x}K_xBiO_3$ (Ref. 3) and the doped fullerenes[4] which have relatively high transition temperatures. This motivates the need for a theory that includes the effects of the so-called vertex corrections, which are neglected in the conventional Migdal-Eliashberg formalism. In this contribution, we present a generalization of the McMillan-Rowell[5] tunneling-inversion program to include the lowest-order effects of vertex corrections in the local approximation, and apply the formalism to the low-temperature superconductor Pb to illustrate how vertex corrections can be incorporated into such an analysis, and to determine, quantitatively, the accuracy of the Migdal-Eliashberg formalism.

The conventional approach to low-temperature three-dimensional superconductors begins with the observation that only the electrons within a thin shell centered about the Fermi surface are affected by the phonons, and if the electronic DOS does not vary within that shell, then one can approximate the electronic band with a constant electronic DOS $\rho(0)$ and hence an infinite bandwidth (the phonons then provide a cutoff to the energy scale). Furthermore, since weak disorder tends to make the gap function isotropic in low-temperature superconductors, the momentum dependence of the electron-phonon matrix elements is also neglected. Then the function $\alpha^2F(\Omega)$ measures the effectiveness of phonons with a frequency Ω in scattering electrons from the Fermi surface onto the Fermi surface and the dimensionless electron-phonon coupling strength is defined to be $\lambda=2\int_0^\infty \alpha^2F(\Omega)/\Omega d\Omega$. We also define $\Omega_{\max}$ to be the maximal phonon frequency where $\alpha^2F(\Omega)$ is nonzero. The Coulomb repulsion is treated by a small pseudopotential μ^* which tends to be a factor of 5 or more smaller than λ in most conventional materials so that higher-order diagrams for the Coulomb interaction can be neglected because $\mu^{*2}\ll 1$. Migdal showed that the electron self-energy is then determined to an accuracy of the order of $\lambda\rho(0)\Omega_{\max}$ when one only includes the set of diagrams where no two phonon lines cross. It is because this so-called Migdal parameter is so small in conventional superconductors that Migdal-Eliashberg theory has been so accurate in describing real materials.

However, motivated by the discovery of newer materials where the Migdal parameter is no longer as small, a systematic study of the effect of the diagrams that Migdal neglected needs to take place. Our philosophy is to include the next most important set of diagrams in the perturbative expansion, i.e., in addition to the usual diagrams in Migdal and Eliashberg's formulation (the set of diagrams where no two phonon lines cross), we also include those diagrams where phonon lines do cross, but the phonon lines only cross in *pairs*. We neglect all diagrams where a phonon line crosses two (or more) other phonon lines. (The Coulomb pseudopotential is

treated in the same way as before, because μ^{*2} is still much smaller than 1. This perturbation theory is valid when Migdal's expansion parameter is moderate, so that those higher-order terms [of order $\lambda^2\rho^2(0)\Omega_{\max}^2$] may be neglected, but is large enough that the effects of the lowest-order vertex corrections are important. It is known, that even in weak coupling (in the limit where $\lambda\to 0$), that these lowest-order vertex corrections *will modify the superconducting T_c by factors of order 1*, and that higher-order vertex corrections will have no effect,[6–9] so a systematic study of just these lowest-order vertex corrections is important. Such a generalization is inadequate for arbitrarily large Migdal parameters, and the only known techniques that can be applied in that case are either a quantum Monte Carlo simulation or an exact-diagonalization study.

Recent work on including the lowest-order vertex corrections into the theory of superconductivity[6–9] has already revealed some of their qualitative effects: If one adopts the conventional approximation of assuming a constant electronic DOS and of neglecting the momentum dependence of the electron-phonon matrix elements, then the vertex corrections will always suppress T_c and the isotope coefficient α. For example, a generalization of the formula for the Holstein model[9] shows that the ratio of the vertex-corrected T_c to the Migdal-Eliashberg T_c is

$$\frac{T_c(\text{vertex})}{T_c(\text{no vertex})}=\exp\left[-\frac{2\pi^2 C\rho(0)}{\lambda}\left(\int_0^\infty d\Omega\,\alpha^2F(\Omega)+\frac{1}{\lambda}\int_0^\infty d\Omega\,\alpha^2F(\Omega)\times\int_0^\infty d\Omega'\,\alpha^2F(\Omega')\frac{1}{\Omega+\Omega'}\right)\right], \tag{1}$$

in the weak-coupling limit with $\mu^*=0$ (C is a dimensionless parameter to be defined in Sec. II). This formula gives an order-of-magnitude estimate for when effects of vertex corrections should be important in a real material (for example, for Pb the ratio is 0.9978 implying a 0.2% effect). Incorporation of either momentum dependence to the matrix elements, or nonconstant electronic DOS can lead to enhancements in T_c and α. Little is known about how large these effects can be in real materials, but they have been verified for model systems by comparing vertex-corrected theories[9] to the exact solution of electron-phonon models in the infinite-dimensional limit.[10]

Even a well-studied low-temperature superconductor such as Pb has a nagging inconsistency between the experimentally extracted $\alpha^2F(\Omega)$ and μ^* and the bulk transition temperature T_c. The extracted dimensionless electron-phonon coupling strength λ satisfies $\lambda=1.55$, and the Coulomb pseudopotential[5] is $\mu^*=0.131$. However, the Coulomb pseudopotential must be increased[11] to $\mu^*=0.144$ in order to produce the correct T_c of 7.19 K. Is it possible that including the vertex corrections can explain this discrepancy since the vertex corrections act like an effective μ^* and suppress T_c?

The organization of this contribution is as follows: In Sec. II, we present the formalism for performing a vertex-corrected tunneling inversion, and we describe the necessary computational methods needed to perform the inversion. In Sec. III, we present results for the vertex-corrected tunneling inversion in Pb. Our conclusions are presented in Sec. IV.

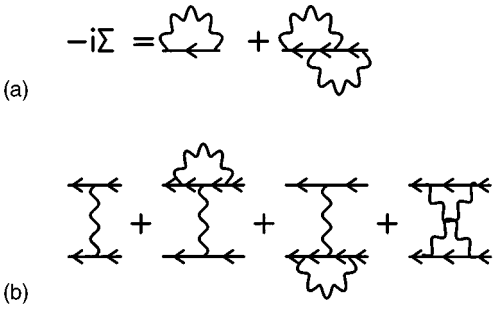

FIG. 1. Feynman diagrams for (a) the electronic self-energy and (b) the irreducible vertex function in the superconducting channel. The first diagram in (a) and (b) is the Migdal-Eliashberg approximation, the remaining diagrams are the lowest-order vertex corrections. The solid lines denote dressed electron propagators and the wavy lines denote dressed phonon propagators.

II. FORMALISM

The first numerical tunneling inversion of a superconductor to determine $\alpha^2F(\Omega)$ and μ^* was performed in the mid 1960's. The calculations were performed directly on the real axis using a sharp cutoff for μ^*. Since then experimentalists have been using essentially the same methods to evaluate their tunneling data. Recently, however, computational strategies have been developed that greatly improve the accuracy of the Migdal-Eliashberg formalism (including placing the sharp cutoff for μ^* on the imaginary axis), and allow for a straightforward generalization to the incorporation of the lowest-order vertex corrections. These new techniques include (i) use of the local approximation for the many-body problem;[12] (ii) performing exact analytic continuations from the imaginary axis to the real axis[13] for electron-phonon systems; and (iii) incorporation of high-frequency resummation schemes[14,15] in order to more properly treat the energy cutoffs. We employ all three strategies in our computational methods.

The electronic self-energy and the irreducible vertex function for superconducting order including the lowest-order vertex correction beyond the conventional model are both illustrated in Fig. 1. The wavy lines denote dressed phonon propagators, and the solid lines denote dressed electronic Green's functions in the Nambu-Gorkov formalism. We make the conventional approximations:[11] (i) neglect the angular dependence of the electron-phonon matrix elements and the phonon spectral functions, and evaluate them at the Fermi energy [this approximation implies that only the function $\alpha^2F(\Omega)$ is needed to determine the coupling of the electrons to the phonons]; (ii) neglect the energy dependence of the electronic density of states $\rho(\epsilon)$ and evaluate it at the Fermi energy $\rho(0)$ [this approximation assumes that the electronic DOS does not vary over the energy scale of the phonons]; and (iii) treat the Coulomb interactions via a pseudopotential for the anomalous self-energy with a sharp cutoff on the imaginary axis [higher-order Coulomb terms are neglected since μ^* is so small]. When these approximations are invoked, one must solve a self-consistent perturbation theory in frequency space only (i.e., a dynamical mean-

field theory)—the self-energy is replaced by a momentum-independent function that has been averaged over the Fermi surface $\Sigma(\omega)=\int\delta(\epsilon_k-\epsilon_F)\Sigma(k,\omega)dk$ (where ϵ_k is the band structure and ϵ_F is the Fermi energy). *These self-consistent equations are identical in form to the equations one would derive in the local approximation, valid in the large-dimensional limit,*[12,9] even though the local approximation would average the self-energy over the entire Brillouin zone, rather than just over the Fermi surface.

The perturbation theory is performed on the imaginary axis at the electronic Matsubara frequencies $i\omega_n:=i\pi T(2n+1)$. It is necessary to make this Wick rotation since a direct evaluation of the vertex-corrected terms on the real axis involves iterated principle-value integrals and is intractable. This also allows for a proper treatment of the Coulomb pseudopotential, since the sharp cutoff lies on the imaginary, not the real axis.[16] If we make the conventional definitions for the quasiparticle renormalization $Z_n:=Z(i\omega_n)=1-\mathrm{Im}[\Sigma(i\omega_n)]/\omega_n$ and for the superconducting gap $\Delta_n:=\Delta(i\omega_n)=\phi(i\omega_n)/Z(i\omega_n)$, then the self-consistent equations are

$$Z_n=1+\frac{\pi T}{\omega_n}\sum_{l=n-N+1}^{n+N}\lambda_l\frac{\omega_{n-l}}{\sqrt{\omega_{n-l}^2+\Delta_{n-l}^2}}+\delta Z_n+\frac{\pi^3T^2C\rho(0)}{\omega_n}\sum_{l=n-N+1}^{n+N}\sum_{l'=n-N+1}^{n+N}\lambda_l\lambda_{l'}\frac{-\omega_{n-l}\omega_{n-l'}\omega_{n-l-l'}-2\omega_{n-l}\Delta_{n-l'}\Delta_{n-l-l'}+\omega_{n-l-l'}\Delta_{n-l}\Delta_{n-l'}}{\sqrt{(\omega_{n-l}^2+\Delta_{n-l}^2)(\omega_{n-l'}^2+\Delta_{n-l'}^2)(\omega_{n-l-l'}^2+\Delta_{n-l-l'}^2)}},\quad(2)$$

$$\Delta_nZ_n=\pi T\sum_{l=n-N+1}^{n+N}(\lambda_l-\mu^*)\frac{\Delta_{n-l}}{\sqrt{\omega_{n-l}^2+\Delta_{n-l}^2}}+\pi^3T^2C\rho(0)\sum_{l=n-N+1}^{n+N}\sum_{l'=n-N+1}^{n+N}\lambda_l\lambda_{l'}\frac{-\Delta_{n-l}\Delta_{n-l'}\Delta_{n-l-l'}-2\Delta_{n-l}\omega_{n-l'}\omega_{n-l-l'}+\omega_{n-l}\omega_{n-l'}\Delta_{n-l-l'}}{\sqrt{(\omega_{n-l}^2+\Delta_{n-l}^2)(\omega_{n-l'}^2+\Delta_{n-l'}^2)(\omega_{n-l-l'}^2+\Delta_{n-l-l'}^2)}},\quad(3)$$

where $\lambda_l:=2\int_0^\infty d\Omega\,\alpha^2F(\Omega)\Omega/(\Omega^2+4\pi^2T^2l^2)$ is the dimensionless electron-phonon coupling, $N=1/2(\omega_c/\pi T-1)$ is the cutoff for the summations [the frequency cutoff is chosen to be six times the maximal frequency in $\alpha^2F(\Omega)$, or $\omega_c=6\Omega_{\max}$], δZ_n is defined below, and C is a Fermi-surface average for the vertex-correction terms. This average is defined by

$$C:=\frac{1}{\rho^4(0)}\sum_q\left[\sum_k\delta(\epsilon_F-\epsilon_k)\,\delta(\epsilon_F-\epsilon_{q-k})\right]^2.\quad(4)$$

The parameter C enters through the summation over momentum in the Feynman diagrams which can be replaced by appropriate averages over the Fermi surface when the momentum dependence of the electron-phonon matrix elements is neglected (the parameter $C=1$ in the local approximation, valid in the large-dimensional limit). In a free-electron model, with a k^2 dispersion, the constant C can be determined analytically, and assumes the form $C=1/6n$, with n the number of electrons per spin per unit cell.[7] Since the DOS at the Fermi level for a free-electron model is $\rho(0)=3n/2\epsilon_F$, the product $C\rho(0)$ is $1/4\epsilon_F$ for this model. For Pb, we perform instead a scalar relativistic density-functional calculation of the band structure in the local-density approximation, and find $\rho(0)=2.5\times10^{-4}$ states/spin/meV, and $C=0.15$, yielding $C\rho(0)=4\times10^{-5}$ states/spin/meV. This is the value we use for the numerical work. Note that it is larger than the free-electron model for Pb, which would predict $C\rho(0)=2.6\times10^{-5}$, mainly because C is enhanced for the true band structure of Pb.

Finally, a high-frequency resummation scheme[14,15] is employed, which calculates the perturbation-theory results relative to the exact results for the normal state, namely,

$$Z_n(\mathrm{normal})=1+\frac{1}{2n+1}\left[\lambda_0+2\sum_{m=1}^{n}\lambda_m\right],\quad(5)$$

by appending the normal-state results to the perturbation theory illustrated in Fig. 1. This is achieved by adding the contribution

$$\delta Z_n:=Z_n(\mathrm{normal})-1-\frac{1}{2n+1}\times\sum_{m=n-N+1}^{n+N}\lambda_m\mathrm{sgn}\left(n-m+\frac{1}{2}\right)\quad(6)$$

[where $\mathrm{sgn}(x)$ is 1 if $x>0$ and -1 if $x<0$] to the perturbation series. The term δZ_n is the normal-state contribution to the quasiparticle renormalization factor that is usually neglected when one introduces the cutoff N into the frequency summations. (Since the form for δZ_n is so simple, the analytic continuation for this contribution can be found exactly in terms of digamma functions as shown in the Appendix.)

The difficult step in the tunneling-inversion program is to analytically continue the gap function to the real axis, in order to determine the tunneling DOS $N(\omega)$ from

$$N(\omega)=N(0)\mathrm{Re}\left[\frac{\omega}{\sqrt{\omega^2-\Delta^2(\omega)}}\right].\quad(7)$$

Recently, however, it was discovered that an exact analytic continuation could be performed by following the prescription of Baym and Mermin:[17] formally perform the analytic continuation $i\omega_n\rightarrow\omega+i\delta$, and then add a function that vanishes at each of the Matsubara frequencies, and is bounded in the upper half-plane except for simple poles located at just

TABLE I. Comparison of fitted tunneling-inversion data for the Migdal-Eliashberg theory and the vertex-corrected theory. The vertex corrections modify λ by the order of 1%.

Theory	λ	$\omega_{\ln}$ (meV)	A (meV)	μ^*	Δ_0 (meV)	T_c (K)	Max. error	RMS error
Migdal-Eliashberg	1.542	4.863	4.029	0.136	1.400	7.23	0.0004	0.0001
Vertex-corrected	1.561	4.847	4.070	0.141	1.400	7.22	0.0007	0.0001

the positions necessary to cancel the poles introduced by the formal analytic continuation. Since the analytic continuation is *unique*, and since the final function can be shown to be analytic in the upper half-plane, this analytic-continuation procedure is exact. Such a scheme has already been implemented for the Migdal-Eliashberg theory,[13] and it is a straightforward but tedious procedure to generalize these results to include the lowest-order vertex corrections. The end result is a formula for the quasiparticle renormalization, and the gap, on the real axis, that involves the data on the imaginary axis and integrals of the Green's function evaluated in the upper half-plane. Explicit formulas appear in the Appendix, since they are cumbersome. Because of the dependence on the Green's function, these equations require a self-consistent solution on a real-axis grid (a step size of 0.05 meV is chosen for the grid spacing). The numerical evaluation of these self-consistent solutions is made difficult by the fact that the integrands can have square-root, or nearly square-root singularities in them. A description of how to numerically evaluate these expressions is included in the Appendix.

Finally, we use this formalism to extract both $\alpha^2F(\Omega)$ and μ^* from the experimental data. We follow the original prescription of McMillan and Rowell:[5] (i) Guess an initial value for $\alpha^2F(\Omega)$. (ii) Adjust μ^* to reproduce the experimental superconducting gap at zero temperature Δ_0 [which is defined from $\mathrm{Re}\Delta(\omega)=\omega$ at $\omega=\Delta_0$]. An analytic continuation employing a Padé approximation is used to determine μ^*, since Δ_0 is determined to an accuracy of one part in 10^5 with such an approximation. (iii) Compute the functional derivative of the change in the tunneling DOS with respect to a change in $\alpha^2F(\Omega)$. (iv) Determine the shift in $\alpha^2F(\Omega)$ by solving the matrix equation

$$\int d\Omega \frac{\delta N(\omega)}{\delta\alpha^2F(\Omega)}\delta\alpha^2F(\Omega)=N(\omega)-N_{\mathrm{exp}}(\omega), \qquad (8)$$

for $\delta\alpha^2F(\Omega)$. This expression is discretized on the real axis, and a singular-value decomposition is employed to determine the shift $\delta\alpha^2F(\Omega)$, since there are small eigenvalues of the functional derivative matrix, which can cause instabilities in updating $\alpha^2F(\Omega)$. (v) Determine the new $\alpha^2F(\Omega)$ by adding a smoothed shift $\delta\alpha^2F(\Omega)$ to it, with $\alpha^2F(\Omega)$ forced to behave quadratically in Ω for $\Omega<0.5$ meV. This procedure is iterated until convergence is reached (typically about ten iterations).

III. RESULTS

The results for the tunneling inversion for Pb for both the Migdal-Eliashberg theory, and the vertex-corrected theory are presented in Table I. Various parameters are recorded including λ, the ''average'' phonon frequency $\omega_{\ln}:=\exp[2\int_0^\infty d\Omega\ln(\Omega)\alpha^2F(\Omega)/(\Omega\lambda)]$, the area A under $\alpha^2F(\Omega)$, μ^*, Δ_0, T_c, the maximum error, and the root-mean-square error of the fit. Note how a proper treatment of the cutoff for μ^* and inclusion of the high-frequency resummation does modify the Migdal-Eliashberg theory tunneling inversion for $\alpha^2F(\Omega)$ by about 0.5% from McMillan and Rowell's results, and improves the calculated T_c (μ^* needs to be increased by 2% to only 0.139 in order to produce the correct bulk T_c of 7.19 K). The vertex corrections modify λ by the order of 1% even though the Migdal parameter $[C\rho(0)\omega_{\max}\lambda]$ is only on the order of 0.0007. The reason why this is so is twofold: first, the tunneling inversion involves the solution of a nonlinear set of equations, in which the effects of the vertex corrections can increase upon each iteration, and second, even if the tunneling data is fit to one part in 10^4, that does not indicate how large the uncertainty is in $\alpha^2F(\Omega)$, since small changes in $\alpha^2F(\Omega)$ can lead to even smaller modifications in the tunneling DOS (especially at higher energies). There is a slight improvement in T_c (μ^* needs to be increased by 1% to 0.143 in order to produce the correct bulk T_c), but it is unlikely that this improvement is significant, based on the quality of the tunneling data itself which is certainly not known to an accuracy of one part in 10^4. A plot of the extracted $\alpha^2F(\Omega)$ is given in Fig. 2(a). The vertex-corrected fit is the solid line and the Migdal-Eliashberg fit is the dashed line. Since these two curves are nearly indistinguishable, the difference between the two spectral functions $\alpha^2F_V(\Omega)-\alpha^2F_{\mathrm{ME}}(\Omega)$ is plotted in Fig. 2(b). The vertex corrections produce slight enhancements to the transverse and longitudinal phonon peaks and they suppress the spectral weight in the region beyond the maximal bulk phonon frequency for Pb (about 9 meV).

We expect the vertex corrections to modify the higher-energy structure in $\alpha^2F(\Omega)$ because they involve processes where two phonons scatter, so that the structures in $\alpha^2F(\Omega)$ are changed at multiples of the lower-energy peaks. We do not see strong evidence of this in the vertex-corrected tunneling inversion of Pb, but that could be because the vertex corrections themselves are so small, that they compete with the nonlinear effects involving the iterated solution of the tunneling-inversion equations. However, this effect could be significant in the recently discovered superconductors.

Finally a comparison of the fitted tunneling DOS is compared to the experimental data[5] in Fig. 3(a). The small dots are the experimental data points used in the fitting procedure; the larger dots (from data taken at a higher temperature) were not used in the fit. The solid line is the vertex-corrected DOS and the dotted line is the Migdal-Eliashberg DOS. Note that the two curves lie on top of each other for low energy, but deviate more at higher energies. In Fig. 3(b), we plot the difference between the Migdal-Eliashberg fit and the experimental data, and similarly for the vertex-corrected theory in Fig. 3(c). Note that the data included in the fit are much more accurate than the data not included. This is in part due to the fact that the higher-energy data were taken at a higher tem-

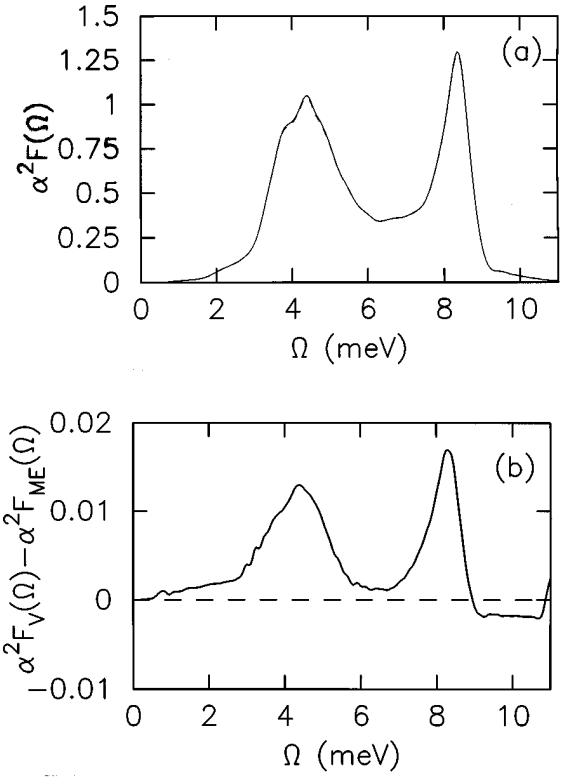

FIG. 2. (a) Electron-phonon spectral function, $\alpha^2F(\Omega)$, extracted from the experimental tunneling data for Pb. The solid line is the vertex-corrected fit and the dashed line is the Migdal-Eliashberg fit. (b) Difference in extracted spectral functions $\alpha^2F_V(\Omega)-\alpha^2F_{ME}(\Omega)$. Note the enhancement of the peaks and the suppression in the region where Ω is larger than the maximum phonon frequency in bulk Pb.

perature than the calculations were performed at. It would be worthwhile to have good quality experimental data out to these energies taken at low temperatures, so that the theory could be unambiguously compared to the experimental results.

IV. CONCLUSION

We have extended the McMillan-Rowell tunneling inversion program to include the lowest-order effect of the vertex corrections. We utilized the local approximation, high-frequency resummations, and an exact analytic continuation from the imaginary axis to the real axis in order to keep the calculations accurate and tractable. We found that the corrections to $\alpha^2F(\Omega)$ and μ^* were larger than expected for Pb, but were still quite small. The main effects were enhancements in the weights of the phonon peaks, and suppression of the weight in the region beyond the maximal bulk phonon frequency.

There are other effects, that have been neglected here, that may cause similar order-of-magnitude corrections in the case of Pb. We have not included any effects due to anisotropy of the gap, or to the momentum dependence of the electron-phonon matrix elements. If those matrix elements have strong momentum dependence, then the formalism presented here would need to be generalized to explicitly include such momentum dependence, and it is likely that the local approximation would no longer be adequate. Such generalization is probably beyond current computational feasibility, but would be necessary if materials were found that display such strong momentum dependence. The results presented here are, however, a necessary first step toward including these momentum-dependent effects, similar to the case of the calculation of T_c for an anisotropic gap, which was achieved by perturbing about the isotropic solutions.[11] In addition, we have not included effects due to nonconstant electronic DOS, nor to lattice anharmonicity. The inclusion of nonconstant DOS is by far the most tractable generalization, since it can be performed using the same formalism, and it is a project that we are currently pursuing.

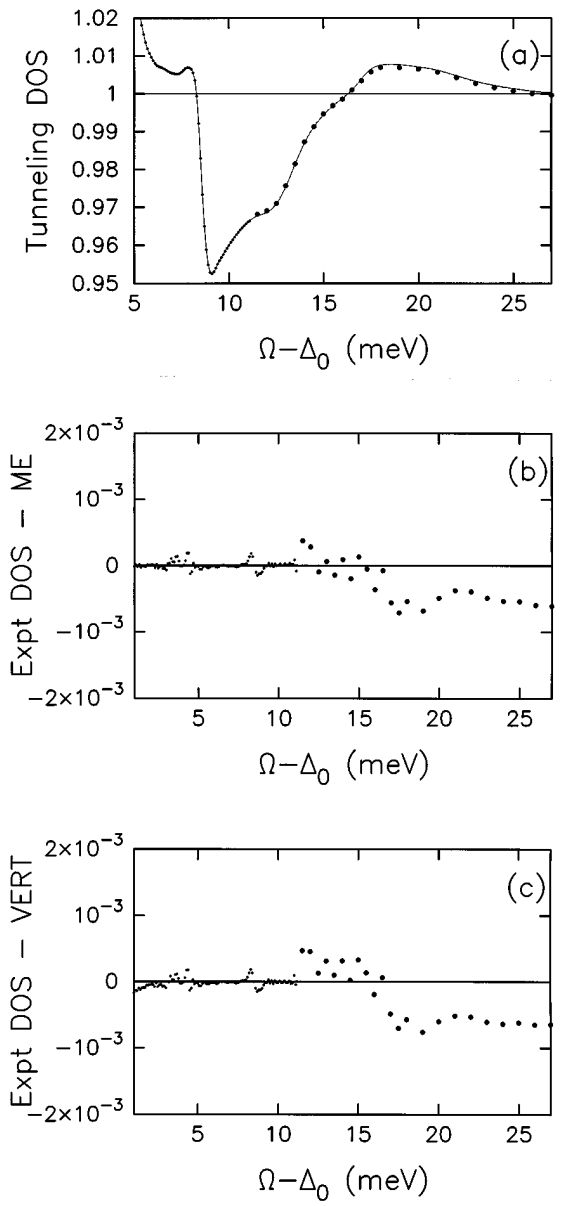

FIG. 3. (a) Comparison of the experimental tunneling DOS (solid dots) to the fitted DOS for Pb. The solid line is the vertex-corrected fit and the dotted line is the Migdal-Eliashberg fit. The small dots are the experimental data included in the fit, while the large dots are experimental data not included in the fit, but taken at a higher temperature (and hence less accurate). (b) Difference between the experimental tunneling DOS and that calculated with the Migdal-Eliashberg theory. (c) Difference between the experimental tunneling DOS and that calculated with the vertex-corrected theory.

Since the fitting procedure for $\alpha^2F(\Omega)$ and μ^* can be an ill-posed problem, we feel that the best way to tackle this problem in the future is to incorporate error bars in the experimental data into the data analysis. Then a maximum-entropy-based tunneling inversion algorithm can be used, where the most probable $\alpha^2F(\Omega)$ and μ^* are determined from the experimental data without trying to fit all experimental data points with equal precision. We hope that more accurate tunneling experiments (including higher-energy data where the vertex corrections are more important) can be performed on well-studied materials such as Pb or Hg, so that the effects of vertex corrections can be demonstrated more easily.

It is possible that effects of vertex corrections could also be seen upon reexamination of isotope coefficient data on low-temperature superconductors. The vertex corrections will act, in general, to reduce α. Work in this direction is currently in progress. We also plan on applying the vertex-corrected tunneling inversion program to both $Ba_{1-x}K_xBiO_3$ and the doped fullerenes, once accurate tunneling data for these materials becomes available.

ACKNOWLEDGMENTS

We would like to acknowledge useful discussions with J. Carbotte, R. Dynes, D. Hess, M. Jarrell, V. Kostur, F. Marsiglio, B. Mitrović, J. Rowell, D. Scalapino, H.-B. Schüttler, and J. Serene. J.K.F. acknowledges the Donors of The Petroleum Research Fund, administered by the American Chemical Society (ACS-PRF No. 29623-GB6) and the Office of Naval Research Young Investigator Program (N000149610828) for partial support of this research. J.K.F. and A.Y.L. acknowledge partial support of the National Science Foundation under Grant No. DMR-9627778. E.J.N acknowledges support from the Natural Sciences and Engineering Research Council of Canada (NSERC).

APPENDIX: DERIVATION OF THE EXACT ANALYTIC CONTINUATION

We begin with a rederivation of the analytic continuation of the Migdal-Eliashberg theory as first described in Ref. 13 based upon the techniques described by Baym and Mermin.[17] We work in the Nambu formalism for the perturbation theory on the imaginary axis

$$\mathbf{G}(i\omega_n):=\begin{pmatrix} G^{\uparrow\uparrow}(i\omega_n) & F(i\omega_n) \\ \overline{F(i\omega_n)} & -G^{\downarrow\downarrow}(-i\omega_n)\end{pmatrix}, \tag{A1}$$

where the diagonal elements $G^{\uparrow\uparrow}$ and $G^{\downarrow\downarrow}$ are the normal Green's functions, and the off-diagonal elements F and F are the anomalous Green's functions. The self-energy (on the imaginary axis) becomes

$$\begin{aligned}\Sigma^{\rm ME}(i\omega_n)&=\frac{T}{\rho(0)}\sum_{l=n-N+1}^{n+N}\lambda(i\nu_l)\tau_3\mathbf{G}(i\omega_n-i\nu_l)\tau_3\\&=\frac{T}{\rho(0)}\sum_{m=-N}^{N-1}\lambda(i\omega_n-i\omega_m)\tau_3\mathbf{G}(i\omega_m)\tau_3,\end{aligned} \tag{A2}$$

where $i\nu_l:=2i\pi Tl$ is the bosonic Matsubara frequency. We substitute in the definition of $\lambda(i\nu_l)$ and formally perform the analytic continuation $i\omega_n\to\omega+i\eta$ with $\eta=0^+$. This yields

$$\Sigma^{\rm ME}(\omega)=-\frac{T}{\rho(0)}\sum_{m=-N}^{N-1}\int_{-\infty}^{\infty}d\Omega\,\alpha^2F(\Omega)\frac{\tau_3\mathbf{G}(i\omega_m)\tau_3}{\omega-i\omega_m-\Omega}+h(\omega), \tag{A3}$$

where $h(\omega)$ is a function that vanishes at each of the fermionic Matsubara frequencies $[h(i\omega_n)=0]$, and is a bounded analytic function in the upper half plane *except* for simple poles that have residues exactly opposite in magnitude to the poles introduced into the upper half plane by the formal analytic continuation. These poles occur at $\omega=\Omega+i\omega_m$ for each value of m in the summation. We choose the functional form

$$f(\omega,\Omega)=\frac{1}{2T}\left[\tanh\frac{\beta}{2}(\omega-\Omega)+\coth\frac{\beta}{2}\Omega\right] \tag{A4}$$

as a function that vanishes when $\omega=i\omega_m$ and has poles with unit residue at $\omega=\Omega+i\omega_m$. We now construct $h(\omega)$ as an integral over $f(\omega,\Omega)$

$$h(\omega)=\frac{T}{\rho(0)}\int_{-\infty}^{\infty}d\Omega\,\alpha^2F(\Omega)\tau_3\mathbf{G}(\omega-\Omega+i\eta)\tau_3f(\omega,\Omega). \tag{A5}$$

This function then has the desired analytic properties, since it is a finite integral [$\alpha^2F(\Omega)$ is a bounded function] of an analytic function $\mathbf{G}$ multiplied by the special function $f(\omega,\Omega)$ which will provide the proper poles, and will vanish at the Matsubara frequencies. The exact analytic continuation becomes

$$\begin{aligned}\Sigma^{\rm ME}(\omega)=&-\frac{T}{\rho(0)}\sum_{m=-N}^{N-1}\int_{-\infty}^{\infty}d\Omega\,\alpha^2F(\Omega)\frac{\tau_3\mathbf{G}(i\omega_m)\tau_3}{\omega-i\omega_m-\Omega}\\&+\frac{1}{\rho(0)}\int_{-\infty}^{\infty}d\Omega\,\alpha^2F(\Omega)\tau_3\mathbf{G}(\omega-\Omega+i\eta)\tau_3\\&\times\frac{1}{2}\left[\tanh\frac{\beta}{2}(\omega-\Omega)+\coth\frac{\beta}{2}\Omega\right],\end{aligned} \tag{A6}$$

which agrees with the known results,[13] but is a simpler derivation. Since the retarded Green's function appears on the right-hand side of the above equation, we must self-consistently solve for the Green's function on the real axis.

The contribution from the high-frequency resummation can also be analytically continued. The contribution to the high-frequency resummation is

$$\begin{aligned}\Sigma^{\rm HF}(i\omega_n)=&-i\pi T\sum_{-\infty}^{\infty}\lambda(i\omega_n-i\omega_m)\mathrm{sgn}(\omega_m)\\&+i\pi T\sum_{m=-N}^{m=N-1}\lambda(i\omega_n-i\omega_m)\mathrm{sgn}(\omega_m),\end{aligned} \tag{A7}$$

which can be analytically continued by using the identity

$$\psi(x)-\psi(y)=\sum_{k=0}^{\infty}\left(\frac{1}{y+k}-\frac{1}{x+k}\right), \tag{A8}$$

in terms of digamma functions. Hence we find

$$\Sigma^{\rm HF}(\omega)=\int_{-\infty}^{\infty}d\Omega\,\alpha^2F(\Omega)\mathrm{Re}\psi\left(\frac{\Omega-\omega}{2i\pi T}+N+\frac{1}{2}\right). \tag{A9}$$

Note that $\alpha^2F(-\Omega)=-\alpha^2F(\Omega)$.

Finally, the vertex-correction terms can also be analytically continued using the same procedure described above. The algebra is more tedious in this case, and the steps will be sketched below: The contribution from the lowest-order vertex-correction to the self-energy is

$$\Sigma^V(i\omega_n)=\frac{CT^2}{\rho^2(0)}\sum_{m=-N}^{N-1}\sum_{m'=-N}^{N-1}\lambda(i\omega_n-i\omega_m)\times\lambda(i\omega_n-i\omega_{m'})\tau_3\mathbf{G}(i\omega_m)\times\tau_3\mathbf{G}(i\omega_m+i\omega_{m'}-i\omega_n)\tau_3\mathbf{G}(i\omega_{m'})\tau_3, \tag{A10}$$

on the imaginary axis. First we introduce the definition of $\lambda(i\nu_l)$ in terms of an integral over $\alpha^2F(\Omega)$; next we use a spectral representation for the middle Green's function

$$\mathbf{G}(i\omega_m+i\omega_{m'}-i\omega_n)=-\frac{1}{\pi}\int_{-\infty}^{\infty}dz\,\frac{\mathrm{Im}\mathbf{G}(z)}{i\omega_m+i\omega_{m'}-i\omega_n-z}, \tag{A11}$$

and then formally perform the analytic continuation to yield

$$\Sigma^V(\omega)=\frac{CT^2}{\rho^2(0)}\sum_{m=-N}^{N-1}\sum_{m'=-N}^{N-1}\int_{-\infty}^{\infty}d\Omega d\Omega' dz\times\frac{\alpha^2F(\Omega)}{\omega-i\omega_m-\Omega}\,\frac{\alpha^2F(\Omega')}{\omega-i\omega_{m'}-\Omega'}\times\frac{\tau_3\mathbf{G}(i\omega_m)\tau_3\mathrm{Im}\mathbf{G}(z)\tau_3\mathbf{G}(i\omega_{m'})\tau_3}{\omega+z-i\omega_m-i\omega_{m'}+i\eta}+h'(\omega). \tag{A12}$$

The function $h'(\omega)$ cancels the poles of the formal analytic continuation in the upper half plane (which occur at $\omega=\Omega+i\omega_m$, $\omega=\Omega'+i\omega_{m'}$, and $\omega=-z+i\omega_m+i\omega_{m'}$), and vanishes at the fermionic Matsubara frequencies. This procedure is exactly the same as performed above, but is more tedious, because the function ultimately involves terms with both single and double integrals of Green's functions evaluated in the upper half plane. The final result is

$$\begin{aligned}\Sigma^V(\omega)=&\frac{CT^2}{\rho^2(0)}\sum_{m=-N}^{N-1}\sum_{m'=-N}^{N-1}\lambda(\omega-i\omega_m)\lambda(\omega-i\omega_{m'})\tau_3\mathbf{G}(i\omega_m)\tau_3\mathbf{G}(-\omega+i\omega_m+i\omega_{m'}-i\eta)\tau_3\mathbf{G}(i\omega_{m'})\tau_3\\
&+\frac{CT}{2\rho^2(0)}\sum_{m=-N}^{N-1}\lambda(\omega-i\omega_m)\int_{-\infty}^{\infty}d\Omega\,\alpha^2F(\Omega)\left[\tanh\frac{\beta}{2}(\omega-\Omega)+\mathrm{cotanh}\frac{\beta}{2}\Omega\right][\tau_3\mathbf{G}(\omega-\Omega+i\eta)\tau_3\\
&\times\mathbf{G}(-\Omega+i\omega_m)\tau_3\mathbf{G}(i\omega_m)\tau_3+\tau_3\mathbf{G}(i\omega_m)\tau_3\mathbf{G}(-\Omega+i\omega_m)\tau_3\mathbf{G}(\omega-\Omega+i\eta)\tau_3]\\
&-\frac{CT}{2\pi\rho^2(0)}\sum_{m=-N}^{N-1}\lambda(\omega-i\omega_m)\int_{-\infty}^{\infty}dz\lambda(-z+i\omega_m)\left[\mathrm{cotanh}\frac{\beta}{2}(\omega+z)-\tanh\frac{\beta}{2}z\right]\tau_3\mathbf{G}(i\omega_m)\tau_3\\
&\times\mathrm{Im}\mathbf{G}(z)\tau_3\mathbf{G}(\omega+z-i\omega_m)\tau_3+\frac{C}{2\rho^2(0)}\int_{-\infty}^{\infty}d\Omega d\Omega'\,\alpha^2F(\Omega)\left[\tanh\frac{\beta}{2}(\omega-\Omega)+\mathrm{cotanh}\frac{\beta}{2}\Omega\right]\alpha^2F(\Omega')\\
&\times\left[\tanh\frac{\beta}{2}(\omega-\Omega')+\mathrm{cotanh}\frac{\beta}{2}\Omega'\right]\tau_3\mathbf{G}(\omega-\Omega+i\eta)\tau_3\mathbf{G}(\omega-\Omega-\Omega'+i\eta)\tau_3\mathbf{G}(\omega-\Omega'+i\eta)\tau_3\\
&-\frac{C}{4\pi\rho^2(0)}\int_{-\infty}^{\infty}d\Omega dz\,\alpha^2F(\Omega)\left[\tanh\frac{\beta}{2}(\omega-\Omega)+\mathrm{cotanh}\frac{\beta}{2}\Omega\right]\lambda(\omega-z-\Omega+i\eta)\left[\mathrm{cotanh}\frac{\beta}{2}(\omega+z)\right.\\
&\left.-\tanh\frac{\beta}{2}z\right]\tau_3\mathbf{G}(\omega-\Omega+i\eta)\tau_3\mathrm{Im}\mathbf{G}(z)\tau_3\mathbf{G}(\Omega+z)\tau_3-\frac{C}{4\pi^2\rho^2(0)}\int_{-\infty}^{\infty}dzdz'\lambda(z'-z)\left[\mathrm{cotanh}\frac{\beta}{2}(\omega+z)\right.\\
&\left.-\tanh\frac{\beta}{2}z\right]\lambda(\omega-z'+i\eta)\left[\tanh\frac{\beta}{2}(\omega+z-z')+\mathrm{cotanh}\frac{\beta}{2}(z'-z)\right]\tau_3\mathbf{G}(\omega+z-z'+i\eta)\tau_3\mathrm{Im}\mathbf{G}(z)\tau_3\mathrm{Im}\mathbf{G}(z')\tau_3.\end{aligned} \tag{A13}$$

Here we have used the notation

$$\lambda(z):=-\int_{-\infty}^{\infty}d\Omega\,\frac{\alpha^2F(\Omega)}{z-\Omega}. \tag{A14}$$

Of course the total self-energy is just

$$\Sigma(\omega)=\Sigma^{\mathrm{ME}}(\omega)+\Sigma^{\mathrm{HF}}(\omega)+\Sigma^V(\omega), \tag{A15}$$

since the sum of these three analytic functions is also an analytic function. Note that the explicit expression for the analytic continuation of the self-energy depends both on the data on the imaginary axis, and on the Green's function evaluated on the real axis, and on lines parallel to the real

axis, but with finite imaginary parts. In order to solve these expressions, we break the real axis up into a grid of points (equally spaced, with a step size of 0.05 meV) and solve for the Green's function at each of these grid points on the real axis. The Green's function in the upper half plane is calculated from a spectral representation as described below.

There are two numerical features that are challenging in the evaluation of these formulas. First, the integrals have square-root, or nearly square-root singularities in them, because the Green's function behaves like

$$G(\omega)\approx\frac{\omega}{\sqrt{\omega^2-\Delta^2(\omega)}}, \tag{A16}$$

and the real part of the denominator vanishes when $\omega=\Delta_0$. Since the imaginary part may be small (it vanishes as $T\rightarrow 0$), the integrals of $G(\omega)$ may have singular (or nearly singular) integrands. We remove the singularities by employing a trigonometric substitution $\omega\rightarrow\Delta_0\sin\theta$ for $|\omega|<\Delta_0$ and $\omega\rightarrow\Delta_0\sec\theta$ for $|\omega|>\Delta_0$. Second, we need the Green's function evaluated along lines parallel to the real axis, but with finite imaginary parts in order to perform the analytic continuation for the vertex-corrected terms. We generate these Green's functions from a spectral representation in the following manner. First, we note that the Green's function can be represented in terms of the gap function $\Delta(\omega)$. The gap function is analytic in the upper half plane, so it can be generated by a spectral representation for $i\Delta(\omega)$ as follows:

$$\begin{aligned} i\Delta(\omega)&=-\frac{1}{\pi}\int_{-\infty}^{\infty}dz\,\frac{\mathrm{Im}[i\Delta(z+i\eta)]}{\omega-z-i\eta}\\ &=i\mathrm{Im}[i\Delta(z_0)]-\frac{1}{\pi}\int_{-\infty}^{\infty}dz\frac{\mathrm{Im}[i\Delta(z+i\eta)-i\Delta(z_0)]}{\omega-z-i\eta}\\ &=i\mathrm{Im}[i\Delta(z_0)]-\frac{1}{\pi}\int_{-\omega^*}^{\omega^*}dz\frac{\mathrm{Im}[i\Delta(z+i\eta)-i\Delta(z_0)]}{\omega-z-i\eta}\\ &\quad-\frac{1}{\pi}\mathrm{Im}[i\Delta_\infty-i\Delta(z_0)]\ln\frac{\omega^*-\omega}{\omega^*+\omega}, \end{aligned} \tag{A17}$$

where z_0 is chosen to be the real part of ω ($z_0=\mathrm{Re}\omega+i\eta$), ω^* is a suitably chosen cutoff (equal to 40 meV for this work), and Δ_∞ is the limiting value of $\Delta(\omega)$ as $\omega\rightarrow\infty$ along the real axis. The middle integral is the only term that needs to be calculated numerically. This procedure yields an accurate result for $G(\omega)$ everywhere in the upper half plane just by using a simple trapezoidal rule for the numerical integration. We found it to be more accurate than using any other spectral representation, since the numerically evaluated integral was small in this case.

[1] A. B. Migdal, Zh. Eksp. Teor. Fiz. **34**, 1438 (1958) [Sov. Phys. JETP **7**, 999 (1958)].

[2] G. M. Eliashberg, Zh. Eksp. Teor. Fiz. **38**, 966 (1960) [Sov. Phys. JETP **11**, 696 (1960)].

[3] L. F. Mattheiss, E. M. Gyorgy, and D. W. Johnson, Jr., Phys. Rev. B **37**, 3745 (1988); R. J. Cava *et al.*, Nature (London) **322**, 814 (1988).

[4] A. F. Hebard *et al.*, Nature (London) **350**, 600 (1991); K. Holczer *et al.*, Science **252**, 1154 (1991); M. J. Rosseinsky *et al.*, Phys. Rev. Lett. **66**, 2830 (1991).

[5] W. L. McMillan and J. M. Rowell, Phys. Rev. Lett. **14**, 108 (1965); in *Superconductivity*, edited by R. Parks (Dekker, New York, 1969), Vol. 1, p. 117.

[6] M. Grabowski and L. J. Sham, Phys. Rev. B **29**, 6132 (1984).

[7] V. N. Kostur and B. Mitrović, Phys. Rev. B **48**, 16 388 (1993); **50**, 12 774 (1994).

[8] L. Pietronero, S. Strassler, and C. Grimaldi, Phys. Rev. B **52**, 10 516 (1995); C. Grimaldi, L. Pietronero, and S. Strassler, *ibid.* **52**, 10 530 (1995); Phys. Rev. Lett. **75**, 1158 (1995).

[9] J. K. Freericks and D. J. Scalapino, Phys. Rev. B **49**, 6368 (1994); J. K. Freericks, *ibid.* **50**, 403 (1994); J. K. Freericks and M. Jarrell, *ibid.* **50**, 6939 (1994); E. J. Nicol and J. K. Freericks, Physica C **235-240**, 2379 (1994); J. K. Freericks, E. J. Nicol, A. Y. Liu, and A. A. Quong, Czech. J. Phys. **46**, Suppl. S2, 603 (1996).

[10] J. K. Freericks, M. Jarrell, and D. J. Scalapino, Phys. Rev. B **48**, 6302 (1993); Europhys. Lett. **25**, 37 (1994); J. K. Freericks and M. Jarrell, Phys. Rev. Lett. **75**, 2570 (1995).

[11] *Superconductivity*, edited by R. Parks (Dekker, New York, 1969); P. B. Allen and B. Mitrović, *Solid State Physics: Advances in Research and Applications*, edited by H. Ehrenreich, F. Seitz, and D. Turnbull (Academic, New York, 1982), Vol. 37, p. 1; J. P. Carbotte, Rev. Mod. Phys. **62**, 1027 (1990).

[12] W. Metzner and D. Vollhardt, Phys. Rev. Lett. **62**, 324 (1989).

[13] F. Marsiglio, M. Schossmann, and J. P. Carbotte, Phys. Rev. B **37**, 4965 (1988).

[14] F. Marsiglio (unpublished).

[15] J. J. Deisz, D. W. Hess, and J. W. Serene, in *Recent Progress in Many-Body Theories*, edited by E. Schachinger *et al.* (Plenum, New York, 1995), Vol. 4, p. 433.

[16] C. R. Leavens and E. W. Fenton, Solid State Commun. **33**, 597 (1980).

[17] G. Baym and N. D. Mermin, J. Math. Phys. **2**, 232 (1961).